Design of a creep resistant nickel base superalloy for power plant applications Part 3–Experimental results

F. Tancret, T. Sourmail, M. A. Yescas, R. W. Evans, C. McAleese, L. Singh, T. Smeeton and H. K. D. H. Bhadeshia

A semi-industrial scale rolled bar of the creep resistant Ni base superalloy designed in Parts 1 and 2 has been fabricated. The influence of heat treatment on microstructure and phase formation has been investigated using both optical and electron microscopy, and X-ray diffraction. Mechanical properties at ambient and high temperature have been measured by hardness testing, compression testing, and tensile creep testing. These experimental results are in good agreement with the predictions of Parts 1 and 2 concerning phase formation, yield stress and creep rupture stress. The target of a lifetime of 100 000 h at 750°C under 100 MPa seems attainable. The design procedure is therefore mainly validated, and results in a promising new alloy for power plant applications. **MST/5391**

Dr Tancret is in the Laboratoire Génie des Matériaux, Polytech' Nantes, La Chantrerie–Rue Christian Pauc, BP 50609, 44306 Nantes Cedex 3, France (franck.tancret@polytech.univ-nantes.fr). Professor Bhadeshia, Dr Sourmail, M. A. Yescas, C. McAleese, L. Singh, and T. Smeeton are in the Department of Materials Science and Metallurgy, University of Cambridge, Pembroke Street, Cambridge CB2 3QZ, UK. Professor Evans is at Swansea IRC, Department of Materials Engineering, University of Wales Swansea, Singleton Park, Swansea SA2 8PP, UK. *Manuscript received 29 January 2002; accepted 18 September 2002.*

Introduction

In Parts 1 and 2 of this present series, the principles behind the design of a new nickel base superalloy (Ni–20Cr–3·5W–2·3Al–2·1Ti–5Fe–0·4Si–0·07C–0·005B (wt-%)) for use in future fossil fuel power plant with steam temperatures as high as 750°C, were described in detail.[1,11,12] This alloy has been proposed on the basis of its estimated mechanical properties (modelled using a Gaussian processes non-linear multi-parameter method),[2] on its predicted phase stability under service conditions (using the Thermo-Calc thermodynamic simulation software), and on processability and cost considerations. This procedure resulted in considerable design cost savings compared with the usual 'try and test' methods.[3] The designed alloy, in which no undesirable phases should form around the service temperature, or due to chemical segregation during casting, should have a creep rupture life of 100 000 h under a stress of 100 MPa at 750°C. It should be resistant to fuel ash corrosion; it should also be forgeable and weldable.

However, before manufacturing or using such an alloy, it requires to be tested thoroughly to see whether it actually behaves in the manner predicted. This also serves to validate the models in domains where they have not previously been applied. Therefore, two 20 kg ingots of the designed material were produced by Special Metals, with a chemical composition within the specified range; the samples were successfully rolled into 30 mm diameter bars. This alloy is still under experimental investigation, and it will be several years before full mechanical properties tests are completed, in particular long term creep rupture tests.

In this work, microstructural and mechanical investigations (including creep tests of more than 4200 h duration) have been carried out on the rolled bar material.

Fabrication and experimental procedures

SEMI-INDUSTRIAL SCALE FABRICATION

Two 20 kg ingots of the designed alloy have been cast by Special Metals, and rolled to the shape of 30 mm diameter cylindrical bars. One of the bars was investigated in this study. The composition of the melt, from chemical analysis, is given in Table 1. It is close to nominal composition except for silicon, but this should not affect the mechanical properties too much. Concerning the strengthening elements, Al, Ti, and W, they are little lower than target; carbon and chromium are slightly higher.

HEAT TREATMENTS

Samples of approximately 10 mm ×6 mm ×5 mm were cut from the bar, and some of them were submitted to one or several heat treatments: they were sealed in quartz tubes under 0·1 bar argon, heated, and then water quenched. The different heat treatments are presented in Table 2.

In the following text, the samples subjected to the last heat treatment of Table 2 are referred to as being 'fully heat treated'.

Rods of about 7·5 cm in length were cut from the bar, submitted to the designed heat treatment directly in the

Table 1 Nominal and actual contents in alloying elements, wt-%

	Cr	W	Al	Ti	Fe	Si	C	B
Nominal	20	3·5	2·3	2·1	5	0·4	0·07	0·005
Actual	20·28	3·308	2·22	1·978	5·025	0·053	0·102	0·0035

Table 2 Effect of heat treatment on grain size and hardness

Heat treatment	Mean linear intercept, μm	Vickers hardness, GPa
As rolled		3·61
1 h at 1150°C	70	1·75
4 h at 1150°C	74	1·70
1 h at 1175°C	159	1·60
4 h at 1175°C	175	1·53
4 h at 1175°C + 4 h at 935°C	…	2·76
4 h at 1175°C + 4 h at 935°C + 24 h at 760°C	…	3·53

 DOI 10.1179/026708303225009805

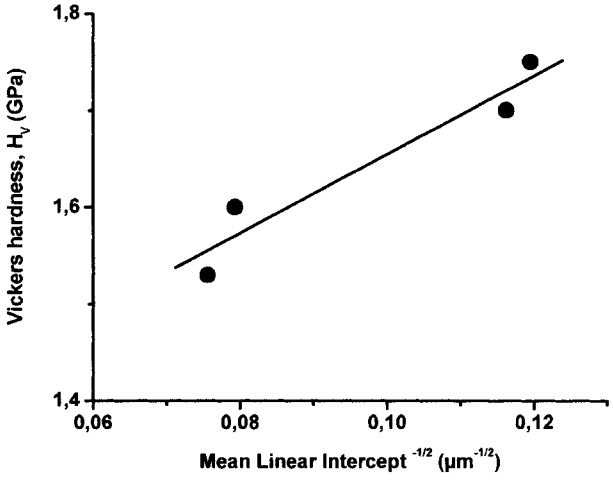

Hall–Petch law

1 Influence of mean linear intercept (representative of grain size) on Vickers hardness in solution heat treated state

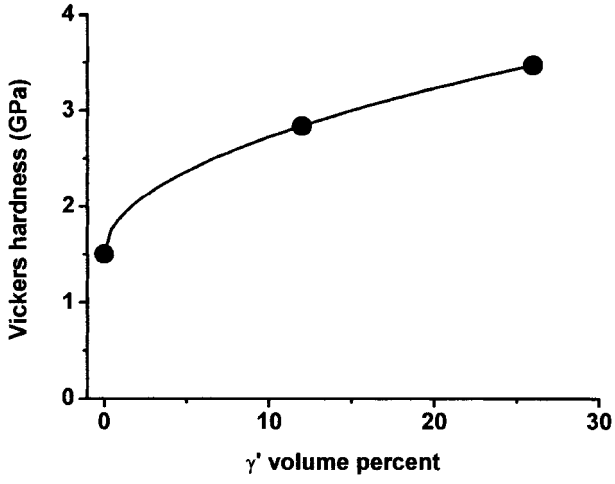

Friedel type law

2 Influence of γ' content on Vickers hardness

furnace without any protection, and then air cooled. They were then cut or machined to the desired shape, depending on the experimental technique to be used.

MICROSTRUCTURE

For microstructural observation, the specimens were mechanically polished using SiC papers down to P1200 grade, then with diamond pastes down to 0·25 μm, and finally chemically etched with a solution of 33 mL HCl, 33 mL ethanol, 33 mL water, and 1·5 g $CuCl_2$. Metallographic observations were carried out using conventional optical microscopy, or using scanning electron microscopy (SEM). The grain size was estimated by the mean linear intercept technique, as measured from between 300 and 600 grains for each sample.

A fully heat treated specimen was cut and then prepared by mechanical grinding followed by electropolishing in a solution of 20% perchloric acid in methanol at 1°C under a potential of 25 V, to be observable using transmission electron microscopy (TEM).

X-RAY DIFFRACTION (XRD)

A fully heat treated and polished specimen was mounted on a rotating stage and investigated using an X-ray diffractometer in the conventional $\theta-2\theta$ geometry, with Cu K_α radiation.

MECHANICAL TESTING

Vickers indentations have been introduced on the surface of polished samples with loads P ranging from 49 N to 196 N, and Vickers hardness H_V has been calculated as

$$H_V = \frac{1{\cdot}854P}{d^2} \quad . \quad . \quad . \quad . \quad . \quad . \quad . \quad . \quad . \quad . \quad . \quad . \quad . \quad (1)$$

where d is the length of the indent diagonal.

For compression testing, cylindrical specimens of approximately 20 mm in length and 8 mm in diameter were cut from the bar using wire erosion, and fully heat treated. Compression tests were carried out on a servohydraulic machine, at ambient and elevated temperatures (25°C, 400°C, 600°C, 800°C, and 900°C, ±2°C), with a crosshead speed of 0·001 mm s^{-1}.

Standard tensile creep testing specimens were machined from fully heat treated rods, with a gauge length of 25·4 mm and a diameter of 5·64 mm. Creep tests were performed in constant stress cam tensile creep machines. Stresses (200 MPa, 230 MPa, 260 MPa, 290 MPa, 320 MPa) could be applied and maintained to an accuracy of 0·5%; a temperature of 750°C was maintained along the gauge length to better than ±0·5 K; creep strains were measured with an accuracy better than 10^{-5} and displacement curves were recorded with approximately 400 points.

Results and discussion

EFFECT OF HEAT TREATMENT ON GRAIN SIZE AND HARDNESS

The effect of the solutionising heat treatment on grain size, and on the annealed state hardness was investigated. Grain size and Vickers hardness values were measured after 1 h or 4 h heat treatment at 1150°C or 1175°C. The results are presented in Table 2.

It can be seen that grain size and hardness respectively increases and decreases as the annealing time and/or temperature is increased. In the studied domain, the effect of temperature is more pronounced than that of time.

Figure 1 reports the variation of hardness as a function of reciprocal of the square root of grain size. The linear regression line shown on the figure corresponds to a classical Hall–Petch law

$$H_V = H_{V0} + kD^{-1/2} \quad . \quad . \quad . \quad . \quad . \quad . \quad . \quad . \quad . \quad . \quad . \quad . \quad (2)$$

where H_{V0} is a reference hardness, D the grain size (here the mean linear intercept), and k a coefficient.

The influence of the different steps of the designed heat treatment on Vickers hardness is presented in Table 2. In the as forged condition, the material is hard, due to its fine grained recrystallised microstructure and probably to some extent due to precipitation hardening. The solution heat treatment of 4 h at 1175°C is expected to destroy this structure and to yield a softer single phase γ material, all the alloying elements being in a metastable solid solution. The measured hardness is actually significantly decreased. The hardness increases as the γ' phase precipitates during the first and second aging treatments at 935°C and 760°C. If it is considered that the phase equilibria predicted in Part 2 are reached during these three heat treatments, the material should contain no γ' after the solution heat treatment, and 12% and 26% of γ' after the first and second aging heat treatments, respectively. In these conditions, the evolution of hardness with γ' volume fraction can be described by a simple Freidel type physical model, as shown on Fig. 2. This model considers the γ' precipitates as dislocations pinning sites, and predicts an increase of the critical shear stress

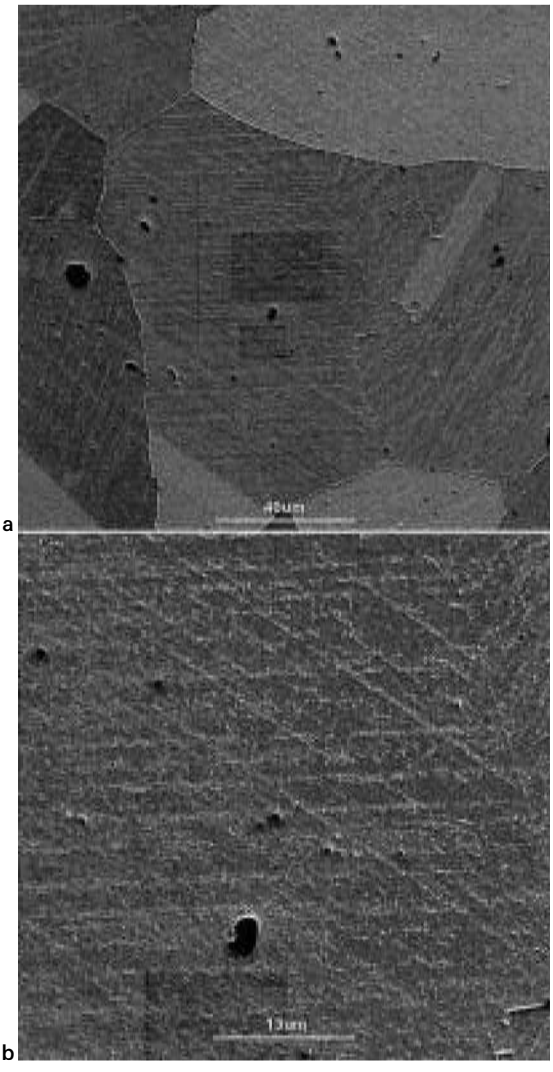

a typical microstructure; *b* $M_{23}C_6$ carbides along stacking faults

3 Scanning electron micrographs of fully heat treated material

$\Delta\tau$ proportional to the square root of the γ' volume fraction V_f as[4]

$$\Delta\tau \propto \sqrt{V_f} \quad . . . . . (3)$$

Although this model is oversimplified because it does not take any interaction between neighbouring precipitates into account and because hardness is not exactly proportional to τ, it gives a good description of the present experimental results.

MICROSTRUCTURE AND PHASE FORMATION IN FULLY HEAT TREATED MATERIAL

A typical SEM micrograph of the fully heat treated alloy is presented in Fig. 3*a*. Large γ grains can be observed, with a series of lines corresponding to stacking faults (Fig. 3*b*), covered with fine $M_{23}C_6$ carbide precipitates, due to the $\gamma \rightarrow \gamma' + M_{23}C_6$ decomposition during cooling. Annealing twins are also seen, as in many Ni base alloys. No chromium rich BCC phase (predicted in Part 2 to appear at low temperatures) was observed.

γ' phase

Spherical γ' precipitates of about 100 nm diameter can be seen on the TEM image shown in Fig. 4. This spherical shape is to be expected for low γ/γ' lattice mismatch alloys.[5]

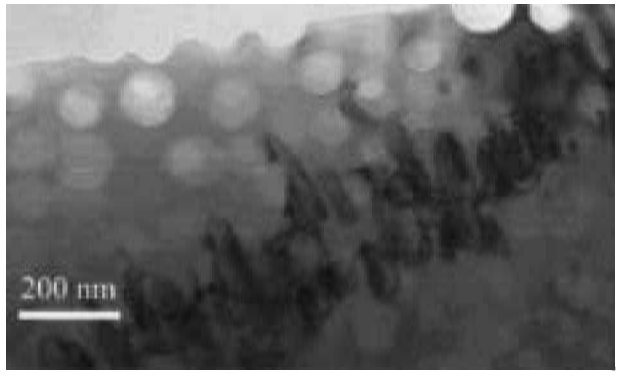

4 Transmission electron micrograph of fully heat treated alloy: spherical γ' inclusions can be seen (light), as well as grain boundary $M_{23}C_6$ carbides (dark)

Attempts were made to measure lattice mismatch and phase volume fractions using X-ray diffraction (Fig. 5). Owing to an actual small lattice mismatch (with ovelapping γ and γ' peaks) and low γ' volume fraction (low γ' peak intensities), it was difficult to calculate precisely the mismatch and the γ' volume fraction. Only the (100) and the (110) γ' peaks could be observed as purely superlattice reflections. Lattice parameters were then estimated to be $a_\gamma = 3{\cdot}581$ Å $\pm 0{\cdot}005$ for γ and $a_{\gamma'} = 3{\cdot}57$ Å $\pm 0{\cdot}01$ for γ', corresponding to a mismatch, defined as $(a_{\gamma'} - a_\gamma)/a_\gamma$, of $-0{\cdot}3 \pm 0{\cdot}4\%$. The predicted Gaussian processes value for lattice misfit at room temperature after quenching from 760°C is $+0{\cdot}3 \pm 0{\cdot}3\%$. Although both techniques are approximate; the predicted and measured values are consistent, since error bars overlap.

Phase volume fractions were also estimated roughly by direct comparison (based on peak intensity measurements) and by a Rietveld fitting analysis. Both techniques give a γ' volume fraction of less than 0·2, whereas the theoretical fraction predicted in Part 2 is 0·26. Nevertheless, TEM observations seem to show that the γ' volume fraction is about right.

An electron diffraction pattern with $[\bar{1}\bar{1}2]$ zone axis, taken from a γ grain containing γ', is shown on Fig. 6, along with its indexed schematic reproduction. The strong spots, represented in the schematic as filled circles, are expected reflections from the γ matrix. In between these, in the $[2\bar{2}0]$ direction are weaker spots (represented as open circles), corresponding to superlattice reflections from the coherent γ' precipitates.

Carbides

Grain boundaries are decorated with particle like $M_{23}C_6$ carbides (Figs. 3 and 4), as expected in the design procedure, which is desirable for good creep resistance. Figure 7 shows the electron diffraction pattern obtained in a grain boundary region, along with its indexed schematic

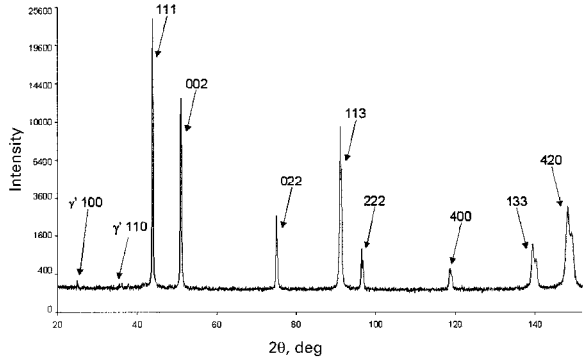

5 Indexed XRD diagram of fully heat treated superalloy

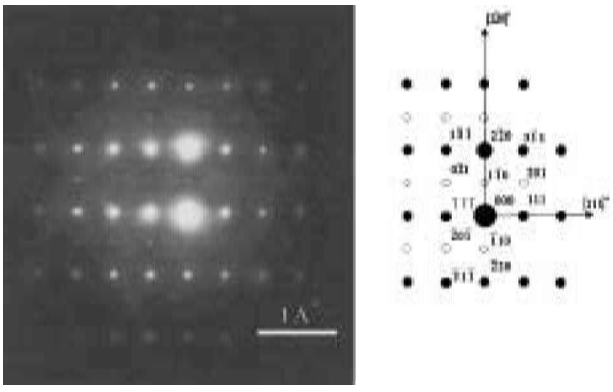

6 **Indexed electron diffraction pattern in γ/γ' area. [$\bar{1}\bar{1}2$] zone axis**

representation. The strongest spots are from the γ matrix and a couple of γ' superlattices have been identified. The remaining spots, represented as grey, filled circles, are assigned to the $M_{23}C_6$ carbides. These carbides could also be observed along stacking faults and twin planes within γ grains.

TiC carbides were also observed, and identified as such by energy dispersive spectroscopy (EDS), although they were not predicted to appear from the thermodynamic simulation of Part 2. Two different kinds of TiC carbides were found, either as isolated particles (Fig. 8*a*), or, more often, around Al_2O_3.MgO spinel inclusions (Fig. 8*b*; also identified using EDS). The last kind of inclusions, of cuboidal shape, form due to reaction between the liquid metal and the furnace ceramics during processing.[6] TiC carbides probably form from the liquid, growing around spinel inclusions or nucleating from the melt. They are known to be stable and difficult to remove by subsequent heat treatment.

MECHANICAL PROPERTIES OF FULLY HEAT TREATED MATERIAL

Yield stress at ambient and high temperatures

A typical stress–strain compression curve is shown in Fig. 9; the strain is measured from the machine extensometer. Yield stresses, measured from the 0·2% plastic deformation offset, are presented as a function of temperature in Fig. 10, and compared to predicted values quoted in Part 1.

Very good agreement between experimental and predicted values is obtained over the whole temperature range. Measured values all lie within prediction error bars. This is a further confirmation that multidimensional non-linear regression techniques, such as Gaussian processes, can be used and relied on to design new materials.

Creep at 750°C

Table 3 gives the testing conditions together with minimum creep rates, times to rupture and creep rupture strains. The test at 200 MPa was unloaded before fracture.

Figure 11 shows the five creep curves obtained. The curves are typical of those to be expected for nickel based alloys. They exhibit a short period of primary creep with no evidence of inverse behaviour. Primary creep is followed by

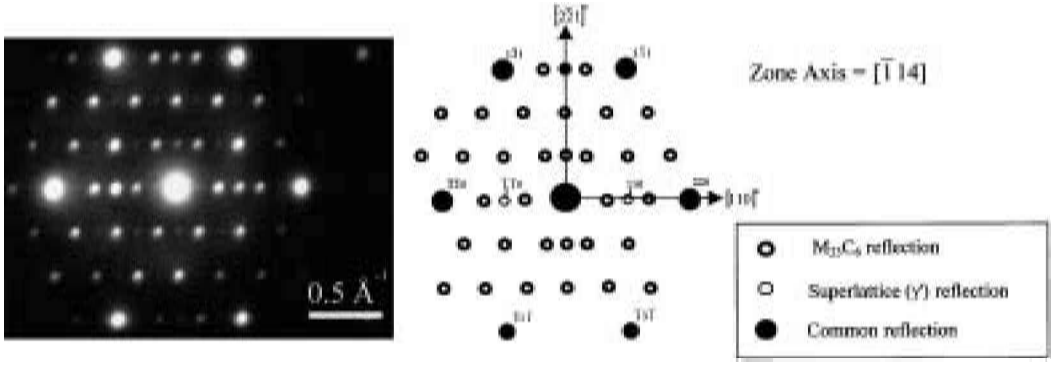

7 **Indexed electron diffraction pattern in grain boundary area**

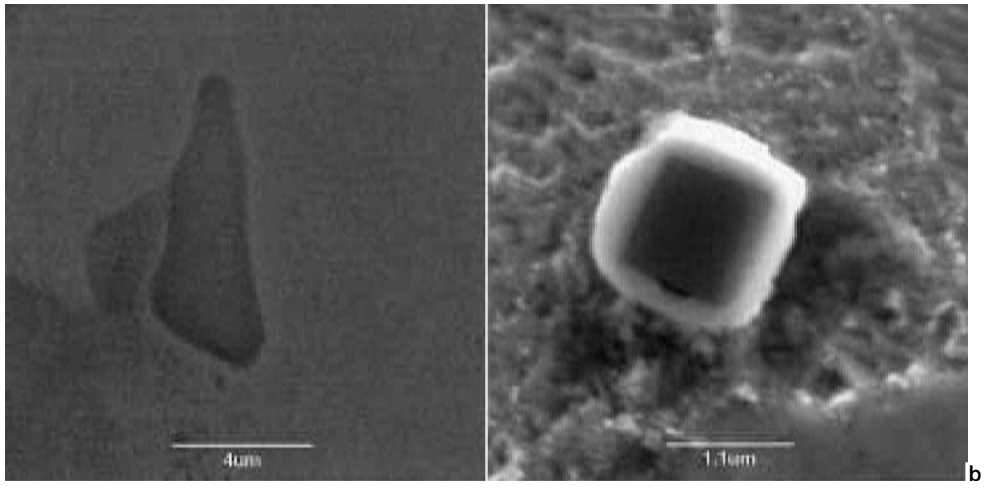

a b

a as a single particle; *b* around a spinel inclusion

8 **Scanning electron microscopic observations of TiC carbides**

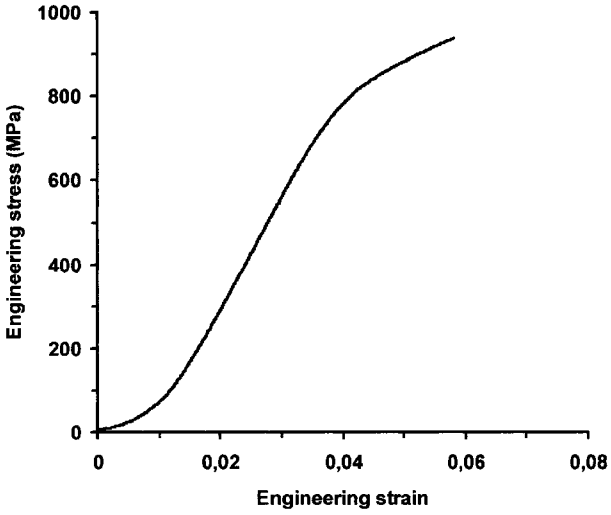

9 Typical stress–strain curve obtained during compression tests at 25°C

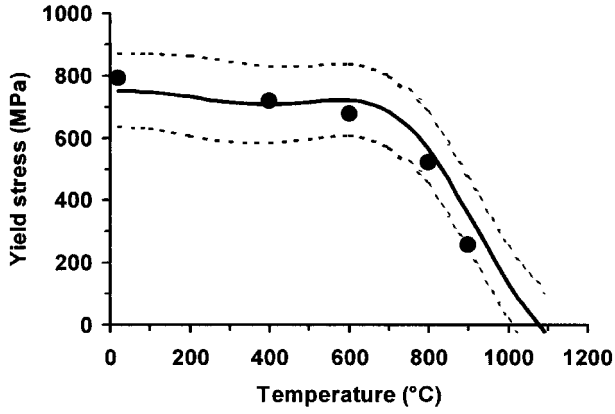

10 Evolution of yield stress as a function of temperature: solid circles indicate measurements; solid line indicates mean Gaussian processes predictions; broken lines indicate predicted error bounds

extensive tertiary deformation, ending in creep rupture. They show the usual behaviour of decreasing minimum creep rate and increasing rupture life with decreasing stress. Rupture strain did not show any significant trend with stress.

Although only four complete tests were available, a single temperature θ projection analysis has been conduced. The θ projection method works in the following way:

- Creep curves under conditions of uniaxial constant stress are measured over a range of stresses and their shapes are estimated.
- These shapes are then projected to other stresses to construct full creep curves, from which creep properties are read.

A single creep curve at steady uniaxial stress τ and absolute temperature T has a shape described by a model function. A variety of model equations have been used to describe the shape of creep curves.[7,8] The equation that has been most widely used and, at least for large strains, has given a good representation of creep curves is

$$\kappa = \theta_1[1-\exp(-\theta_2 t)] + \theta_3[\exp(\theta_4 t)-1] \quad . \quad . \quad . \quad . \quad . \quad (4)$$

where κ is the uniaxial creep strain at time t and θ_j are numerical parameters that can be determined from the experimental creep curves. For a series of experimental creep curves obtained under different conditions, the θ_j are related to τ by interpolation functions, chosen as

$$\ln \theta_j = b_{j1} + b_{j2}\tau \quad . \quad . \quad . \quad . \quad . \quad . \quad . \quad . \quad . \quad . \quad . \quad (5)$$

Table 3 Conditions and results of creep tests at 750°C: index letter denotes specimen rupture (R) or interrupted test (I)

Stress, MPa	Minimum creep rate, s^{-1}	Final time, h	Final strain, %
320	$8{\cdot}33\times10^{-8}$	118_R	$5{\cdot}05_R$
290	$2{\cdot}77\times10^{-8}$	412_R	$4{\cdot}46_R$
260	$8{\cdot}35\times10^{-9}$	756_R	$6{\cdot}15_R$
230	$2{\cdot}27\times10^{-9}$	2290_R	$4{\cdot}85_R$
200	$7{\cdot}58\times10^{-10}$	4277_I	$1{\cdot}70_I$

In these functions, j is the subscript identifying θ in equation (4) and b_{jk} are constants determined by a suitable regression procedure. Equation (5) permits the projection of θ_j to new conditions of stress and hence construction of the appropriate creep curve. The method has yielded excellent results for moderate to large creep strains. The method is described in more detail in Ref. 9.

The θ_j in equation (4) have been estimated from experimental creep curves by a non-linear least squares procedure described elsewhere.[10] Values of the constants in the interpolation functions were determined by linear least squares procedures with the θ_j weighted by their variances.

In a similar way, the rupture strains κ^f were related to stress by the logarithmic function

$$\ln(\kappa^f) = b_{f1} + b_{f2}\tau \quad . \quad . \quad . \quad . \quad . \quad . \quad . \quad . \quad . \quad . \quad . \quad (6)$$

Table 4 lists the interpolation coefficients for θ_j and κ^f.

Figures 12, 13 and 14 show the projected values of the minimum creep rate, rupture time and rupture ductility together with the experimental values for the alloy. Where possible, the graphs include 95% confidence intervals for the predictions. Figure 12 includes the experimental minimum creep rate at 200 MPa although this test was not used in the θ analysis. The rate corresponds well with the extrapolated value. It thus becomes possible to use this θ projection technique to extrapolate the rupture time and ductility under a stress of 200 MPa. The values obtained in this way using extraploation are 4626 h ($\pm$ 260) and 3·67%, respectively.

Measured rutpure times for stresses of 320, 290, 260, and 230 MPa, as well as the extrapolated value for 200 MPa and the Gaussian processes predictions of Part 1, are plotted as a stress–lifetime graph in Fig. 15. Excellent agreement is obtained between predictions and experiments, which gives confidence in the statement that the alloy is likely to meet the intended engineering target of 100 000 h under 100 MPa at 750°C. For comparison purposes, the estimated 1000 h creep rupture stress of the designed alloy at 750°C is about 240 MPa, which is close to the estimated values for some commercial alloys: about 230 MPa for Alloy 901, Inconel 718, and Nimonic 90. All these alloys contain Mo, Co and/or Nb, which makes their elemental price higher, and they contain less Cr than the designed alloy, which makes them less resistant to corrosion.

Table 4 Interpolation coefficients for θ_j and ξ^f

	θ_1	θ_2	θ_3	θ_4	κ^f
b_1	−9·74080	−11·6441	−8·97229	−19·7635	0·405431
b_2	$9{\cdot}70282\times10^{-3}$	$1{\cdot}18377\times10^{-2}$	$2{\cdot}05718\times10^{-2}$	$1{\cdot}84146\times10^{-2}$	$-1{\cdot}45269\times10^{-3}$

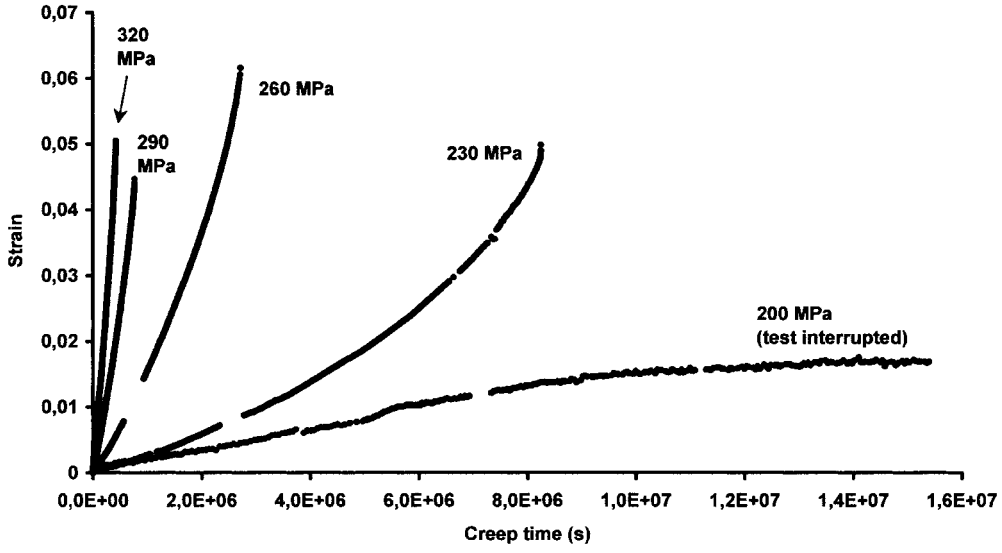

11 Creep curves at 750°C of fully heat treated alloy

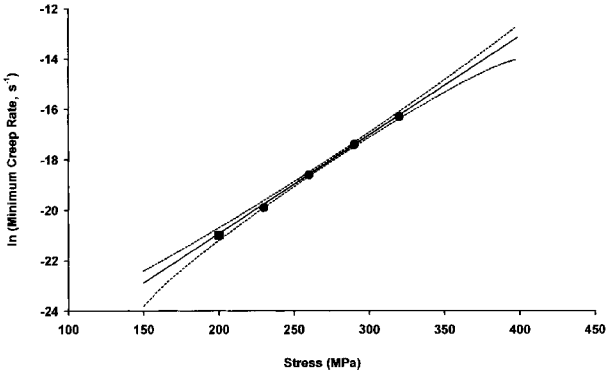

12 Minimum creep rate as function of stress: symbols are measured values; solid line interpolated and extrapolated values; broken lines 95% confidence intervals

Conclusions

A semi-industrial scale rolled bar of a newly designed Ni base superalloy has been fabricated and submitted to microstructural, structural, and mechanical investigations, using optical microscopy, TEM, XRD, Vickers hardness testing, compression testing, and tensile creep testing.

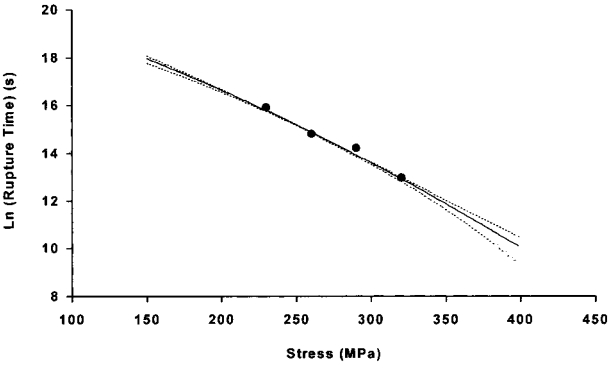

13 Creep rupture time as function of stress: symbols are measured values; solid line interpolated and extrapolated values; broken lines 95% confidence intervals

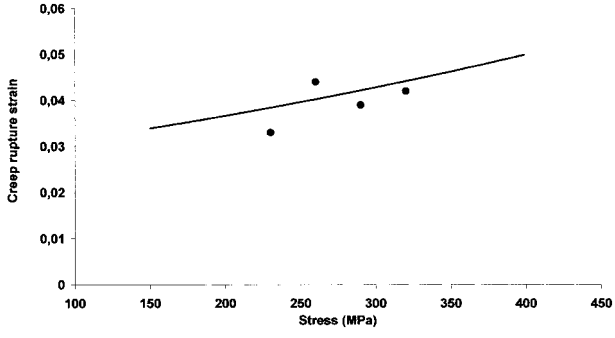

14 Creep rupture strain as a function of stress: symbols are measured values; solid line interpolated and extrapolated values

The expected influence of solution and aging heat treatments on grain size and hardness could be observed and described by simple theoretical models (Hall – Petch for the effect of grain size and Friedel for precipitation strengthening). Microstructural and structural characterisations confirmed that the structure of the fully heat treated alloy is close to that expected from both thermodynamical simulation and simple metallurgical considerations: approximately

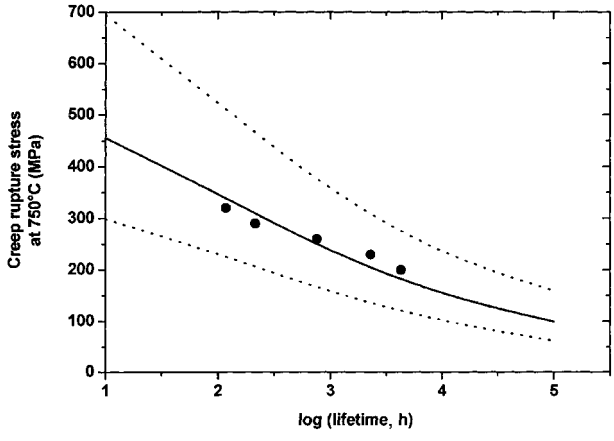

15 Evolution of creep rupture stress as function of temperature: solid circles indicate measurements; solid line indicates mean Gaussian processes predictions; broken lines indicate predicted error bounds

20 vol.-% γ' embedded in γ grains with a small lattice mismatch, and particle like $M_{23}C_6$ carbides mainly present at grain boundaries. Also, measured mechanical properties (yield stress at ambient and high temperatures and creep at 750°C) on the fully heat treated material are in good agreement with the values predicted by the Gaussian processes models developed in Part 1. Although extrapolation can be uncertain, it is believed that the designed alloy will match the engineering criterion of a creep rupture time of 100 000 h under 100 MPa at 750°C.

Acknowledgements

The authors are grateful to the Engineering and Physical Sciences Research Council for funding this work, and to Alstom Power, Corus, Mitsui Babcock Energy Ltd., Rolls-Royce plc, and Special Metals, for partnership. The authors thank Professor Colin Humphreys for all his support in the Technology Foresight Programme.

References

1. F. TANCRET, H. K. D. H. BHADESHIA and D. J. C. MACKAY: *Key Eng. Mater.*, 2000, **171–174**, 529–536.
2. F. TANCRET, H. K. D. H. BHADESHIA and D. J. C. MACKAY: *ISIJ Int.*, 1999, **39**, 1020–1026.
3. F. TANCRET: in 'Processing for China', 56–58; 2000, London, Sterling Publications.
4. J. FRIEDEL: 'Dislocations'; 1964, Oxford, Pergamon Press.
5. A. MAHESHWARI and A. J. ARDELL: *Scr. Metall. Mater.*, 1992, **26**, 347–352.
6. M. DURANDCHARRE: 'The microstructure of superalloys'; 1997, Amsterdam, Gordon and Breach.
7. A. GRAHAM and K. F. A. WALLES: *J. Iron Steel Inst.*, 1955, **193**, 105.
8. F. GARAFALO, C. RICHMOND, W. F. DOMIS and F. VON GEMMINGEN: Proc. Joint. Int. Conf. on 'Creep', London, 1965, Institute of Mechanical Engineers.
9. R. W. EVANS: *Proc. R. Soc. (London) A*, 2000, **A456**, 835.
10. R. W. EVANS: *Mater. Sci. Technol.*, 1989, **5**, 699.
11. F. TANCRET, H. K. D. H. BHADESHIA and D. J. C. MACKAY: *Mater. Sci. Technol.*, 2003, **19**, 283–290.
12. F. TANCRET, H. K. D. H. BHADESHIA and D. J. C. MACKAY: *Mater. Sci. Technol.*, 2003, **19**, 291–295.